Available online at www.sciencedirect.com

ScienceDirect

Nuclear Physics A 1038 (2023) 122719

NUCLEAR PHYSICS A

www.elsevier.com/locate/nuclphysa

# Neutrino-induced reactions on $^{18}$O and implications of $^{18}$O mixture in water Cherenkov detectors on supernova neutrino events

Toshio Suzuki [a,b,c,*], Ken'ichiro Nakazato [d], Makoto Sakuda [e]

[a] *NAT Research Center, 3129-45 Hibara Muramatsu, Tokai-mura, Naka-gun, Ibaraki 319-1112, Japan*
[b] *Department of Physics, College of Humanities and Sciences, Nihon University, Setagaya-ku, Tokyo 156-8550, Japan*
[c] *School of Physics, Beihang University, 37 Xueyuan Road, Haidian-qu, Beijing 100083, People's Republic of China*
[d] *Faculty of Arts and Science, Kyushu University, Fukuoka 819-0395, Japan*
[e] *Physics Department, Okayama University, Okayama 700-8530, Japan*

Received 30 May 2023; received in revised form 3 July 2023; accepted 4 July 2023
Available online 10 July 2023

**Abstract**

Neutrino-nucleus reaction cross sections on $^{18}$O are evaluated by shell-model calculations and compared with those on $^{16}$O. Important contributions from Gamow-Teller transitions are noticed for $^{18}$O ($\nu_e$, e$^-$) $^{18}$F in contrary to the case for $^{16}$O, where spin-dipole transitions are dominant contributions. Calculated cross sections for $^{18}$O ($\nu_e$, e$^-$) $^{18}$F are shown to be larger than for $^{16}$O at low neutrino energies below 20 MeV in natural water with the 0.205% admixture of $^{18}$O due to the lower threshold energy (1.66 MeV) for $^{18}$O than that for $^{16}$O (15.42 MeV). The resulting electron spectra, that is, the cross sections as functions of emitted electron energy $T_e$, are also shown to be quite different, reflecting the different threshold energies. The electron spectra from ($\nu_e$, e$^-$) reactions on $^{18}$O and $^{16}$O in water Cherenkov detectors for supernova neutrino detection are investigated for both the cases with and without the neutrino oscillation and compared with those of the neutrino-electron scattering. It has been shown that the contribution from $^{18}$O (0.205% mixture) enhances the rates from $^{16}$O by 60% for the case without the oscillation and by 20-30% for the case with the oscillation below $T_e$ =20 MeV. For the case with the neutrino oscillation, the event rates for $^{18}$O and $^{16}$O become comparable to those of the neutrino-electron scattering. However, their rates at low energy ($T_e < 20$ MeV) are much lower than those of the neutrino-electron scattering, which is important for the pointing accuracy to the supernova direction.


* Corresponding author.
*E-mail address:* suzuki.toshio@nihon-u.ac.jp (T. Suzuki).

https://doi.org/10.1016/j.nuclphysa.2023.122719
0375-9474/

*Keywords:* Neutrino-nucleus reactions; Shell model; Gamow-Teller transition; Supernova neutrinos; Water Cherenkov detector; Neutrino oscillation

## 1. Introduction

Water Cherenkov detectors are powerful tools to probe supernova neutrinos and study their properties. Super-Kamiokande has been searching for neutrino bursts characteristic of core-collapse supernovae continuously, in real time, since the start of operations in 1996 [1]. Hyper-Kamiokande [2] is planned to determine the neutrino mass hierarchy and CP-violating phase as well as the supernova explosion mechanism [3,4]. Long-term (up to $\sim$10 s after the collapse) measurement of supernova neutrinos produced in the neutronization burst, the accretion phase, and the cooling phase can provide information on the nature of progenitor and remnant. The neutrino luminosity in the accretion phase is determined by the progenitor model, while the signal in the cooling phase could provide hints for the mass of the remnant neutron star [4]. Both charged-current and neutral-current neutrino-nucleus reactions on $^{16}$O have been studied by shell model [5] and CRPA calculations [6]. Dominant contributions to the cross sections come from spin-dipole (SD) transitions. The SD strengths, charged- and neutral-current total and partial reaction cross sections for various particles and $\gamma$ emission channels have been evaluated with the Hauser-Feshbach statistical model [5,6].

Here, we study $\nu$-induced reactions on $^{18}$O, which has isotope abundance of 0.205%. Gamow-Teller (GT) transitions give considerable contributions to the charged-current reaction cross sections for $^{18}$O ($\nu_e$, e$^-$) $^{18}$F. Experimental data for the GT strength in $^{18}$O was obtained by ($^3$He, $t$) reactions on $^{18}$O [7]. Cross sections for $^{18}$O ($\nu_e$, e$^-$) $^{18}$F are evaluated with the use of an effective axial-vector coupling constant $g_A^{eff}$ determined from the experimental GT strength.

Charged-current reaction $^{18}$O ($\nu_e$, e$^-$) $^{18}$F caused by the admixture of $^{18}$O in natural water was calculated previously and pointed out to account for about 10% of electron events induced by solar neutrinos generated by $^8$B $\beta$ decay [8]. Elastic $\nu$-$e^-$ scattering is the main source of electron events. Taking account of the isotopic abundance of $^{18}$O, the sum of $\nu$-induced reaction cross sections on $^{16}$O and $^{18}$O were evaluated for supernova spectra, which were taken to be Fermi-Dirac distributions with temperatures $T$ = 3-10 MeV [8]. The temperature of $\bar{\nu}_e$ was suggested to be $T_{\bar{\nu}_e}$ = 4-5 MeV from the measurement of SN1987A neutrinos at Kamioka [9] and IMB [10], but no observational information was available for the temperatures of $\nu_e$ and $\nu_x$ where $x = \mu$, $\tau$ or $\bar{\mu}$, $\bar{\tau}$. There were fairly large uncertainties in the supernova neutrino spectra. Supernova model calculations lead to a hierarchy for the temperatures, $T_{\nu_e} \leq T_{\bar{\nu}_e} < T_{\nu_x}$, where $T_{\nu_x}$ was predicted to be as high as 8 MeV [11]. The nucleosynthesis of elements produced by $\nu$-processes was studied with the use of temperatures that satisfy this hierarchy; ($T_{\nu_e}$, $T_{\bar{\nu}_e}$, $T_{\nu_x}$) = (3.2, 5, 8) MeV [12] or (4, 4, 8) MeV [13]. A lower temperature for $T_{\nu_x} \approx$ 6 MeV was pointed out to be favored from constraints on the abundance of $^{11}$B obtained by $\nu$-process and galactic chemical evolution [14,15]. The observed solar-system abundances of $\nu$-process elements, $^{138}$La and $^{180}$Ta, are found to be consistently reproduced by taking $T_{\nu_e} \approx T_{\bar{\nu}_e} = 4$ MeV [16,17]. While temperatures of the Fermi distributions have been updated, another analytical form for the neutrino spectra called modified Maxwell-Boltzmann distribution was proposed [18] and became more commonly used than the Fermi distributions. The modified Maxwell-Boltzmann distribution has two characteristic parameters, which are average energy and spectral pinching. Recent supernova models lead to spectra with smaller average energy for $\nu_x$, that is, $T_{\nu_x} \approx T_{\bar{\nu}_e}$, but with large high energy components produced in the accretion phase of

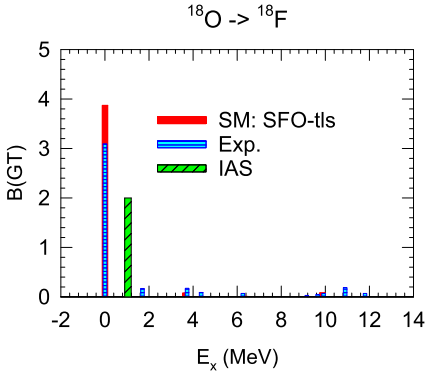


Fig. 1. Gamow-Teller strengths obtained by shell-model calculations with the use of SFO-tls and experimental data [7] are shown by red solid and blue hatched histograms, respectively. The quenching factor for $g_A$ is taken to be $q = 0.88$. Green dashed histogram denotes Fermi contributions, $B(F)$, from the transition to the isobaric analog state (IAS), $^{18}$F ($0^+$, 1.04 MeV, $T = 1$). (For interpretation of the colors in the figure(s), the reader is referred to the web version of this article.)

the supernova explosions [4,19,20]. Here, possible effects of the $^{18}$O mixture on the count rate of supernova $\nu$ events in water Cherenkov detectors are examined with the use of recent realistic neutrino spectra. Effects of neutrino oscillations, which exchange $\nu_e$ and $\nu_x$, on the count rate are also investigated.

In Sect. 2, the GT strength in $^{18}$O is obtained by shell-model calculations and compared with the experimental data. Then, $\nu$-induced reaction cross sections for $^{18}$O are evaluated for both charged- and neutral-current channels, and compared with those for $^{16}$O. Event spectra for emitted electrons induced by reactions in natural water are also examined. In Sect. 3, contributions of $^{18}$O mixture to the count rate of supernova $\nu$ events in water Cherenkov detectors are estimated. The summary is given in Sect. 4.

## 2. $\nu$-induced reactions on $^{18}$O

### 2.1. Gamow-Teller strength in $^{18}$O

We first evaluate GT strength in $^{18}$O by shell-model calculations with the use of SFO-tls Hamiltonian [21] in *p-sd* shell. The Hamiltonian, SFO-tls, was used to obtain $\nu$-induced reaction cross sections in $^{16}$O [5]. The $B(GT_\pm)$ is defined as

$$B(GT_\pm) = \frac{1}{2J_i+1}|\langle f||q\sum_k \vec{\sigma}_k t^k_\pm||i\rangle|^2 \tag{1}$$

where $J_i$ is the spin of the initial state, $t_-|n\rangle = |p\rangle$, $t_+|p\rangle = |n\rangle$ and $q$ is the quenching factor for the axial-vector coupling constant, $q = g_A^{eff}/g_A$. The sum runs over all nucleons. The quenching factor is determined to reproduce the experimental sum of the strength, $S = 4.06$, measured up to the excitation energy $E_x = 12$ MeV. It is obtained to be $q = 0.88$. Calculated $B(GT_-)$ and the experimental data [7] are shown in Fig. 1.

The GT transitions from the ground state of $^{18}$O ($0^+$, $T = 1$) to the $1^+$ states in $^{18}$F with isospin $T = 0$, 1 and 2 contribute to the cross sections. A large strength is noticed for the transi-

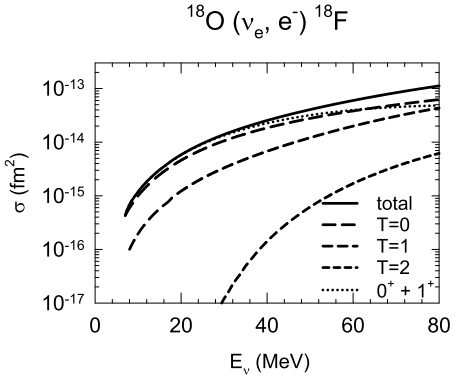


Fig. 2. Calculated cross sections for $^{18}$O ($\nu_e$, e$^-$) $^{18}$F. The solid curve shows the total cross section. Long-dashed, dashed, and short-dashed curves denote its components of transitions to the states with $T = 0$, 1, and 2, respectively. The dotted curve shows the sum of cross sections for the GT ($1^+$) and Fermi ($0^+$) transitions.

tion to the ground state of $^{18}$F ($1^+$, $T = 0$). The strength of the Fermi transition, $B(F)$, is defined as

$$B(F) = \frac{1}{2J_i + 1} |\langle f || \sum_k t_-^k || i \rangle|^2. \tag{2}$$

The value of the $B(F)$ for the transition to the isobaric analog state (IAS), $^{18}$F ($0^+$, 1.04 MeV, $T = 1$) is equal to 2. Note that the isospin of the final states is $T = 1$ or 2 and only $T = 2$ for the transitions to $^{18}$O and $^{18}$N, respectively. The transition strengths for $^{18}$O and $^{18}$N are, therefore, suppressed compared to the strength for $^{18}$F.

### 2.2. Reaction cross sections for $^{18}O$

In this subsection, reaction cross sections for $^{18}$O ($\nu_e$, e$^-$) $^{18}$F, $^{18}$O ($\bar{\nu}_e$, e$^+$) $^{18}$N and $^{18}$O ($\nu$, $\nu'$) $^{18}$O are evaluated by shell-model calculations in *p-sd* shell with the use of SFO-tls. Configurations up to 2p-2h (3p-3h) excitations are included for positive (negative) parity states. The cross sections are obtained by using the multipole expansion of the weak hadronic currents,

$$J_\mu^{C_\mp} = J_\mu^{V_\mp} + J_\mu^{A_\mp} \tag{3}$$

for charged-current reactions ($\nu_e$, e$^-$) and ($\bar{\nu}_e$, e$^+$), and

$$J_\mu^N = J_\mu^{A_3} + J_\mu^{V_3} - 2\sin^2\theta_W J_\mu^\gamma \tag{4}$$

for neutral-current reactions, ($\nu$, $\nu'$) and ($\bar{\nu}$, $\bar{\nu}'$), where $J_\mu^V$ and $J_\mu^A$ are vector and axial-vector currents, respectively, and $J_\mu^\gamma$ is the electromagnetic vector current with $\theta_W$ the Weinberg angle. The reaction cross sections are given as the sum of the matrix elements of the Coulomb, longitudinal, and transverse electric and magnetic multipole operators for the vector and axial-vector currents [22,23]. Here, all the transition matrix elements with multipolarities up to $\lambda = 4$ are taken into account with the use of harmonic oscillator wave functions. The quenching factor for $g_A$ determined in Sect. 2.1, $q = 0.88$, is used for all the multipoles. Calculated results are shown in Fig. 2 as functions of neutrino energy $E_\nu$. We note that the contributions from the GT ($1^+$) and Fermi ($0^+$) transitions are dominant at $E_\nu < 40$ MeV, and the transitions to the states with

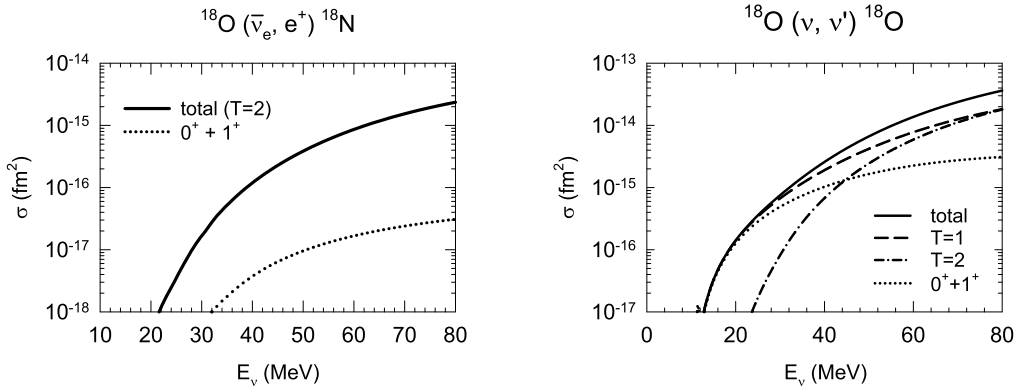


Fig. 3. Calculated reaction cross sections for $^{18}$O ($\bar{\nu}_e$, e$^+$) $^{18}$N (left panel) and $^{18}$O ($\nu$, $\nu'$) $^{18}$O (right panel). Total cross section and the sum of cross sections for $0^+$ and $1^+$ multipoles are shown. Final states of $^{18}$N have isospin $T = 2$, while those of $^{18}$O have $T = 1$ and 2.

isospin $T = 0$ are most important. The $T = 0$ component is mostly the GT transitions, and the $T = 1$ component is dominantly the Fermi transition to the IAS state. Spin-dipole transitions are the dominant contributions to the $T = 2$ component. The calculated total cross section is found to be larger than that for $^{16}$O as will be shown in Sect. 2.3.

Cross sections for ($\bar{\nu}_e$, e$^+$) and ($\nu$, $\nu'$) reactions are also evaluated by the multipole expansion method, and the results are shown in Fig. 3. The calculated cross sections are smaller than those for the ($\nu_e$, e$^-$) reaction by more than one order of magnitude because there are no first-order allowed GT transitions to $T = 0$ states, that are present in the ($\nu_e$, e$^-$) reaction channel. Note also that the transition to the IAS state ($0^+$, $T = 1$) does not exist in the ($\bar{\nu}_e$, e$^+$) and ($\nu$, $\nu'$) reactions. Large threshold energy for the ($\bar{\nu}_e$, e$^+$) reaction further suppresses the magnitude of the cross section.

### 2.3. Comparison with reaction cross sections for $^{16}$O

Now, we compare the cross sections for $^{18}$O with those for $^{16}$O. The calculated total cross sections for $^{18}$O ($\nu_e$, e$^-$) $^{18}$F are compared with those for $^{16}$O ($\nu_e$, e$^-$) $^{16}$F in Fig. 4 (left panel). Here, the quenching factor for $g_A$ for $^{16}$O is taken to be $q = 0.68$ (dotted curve) for the transitions to the first $0^-$, $1^-$ and $2^-$ states in $^{16}$F [24], which was determined by fitting to the experimental $\mu$-capture rates (see Ref. [24] for the details). For transitions to other states in $^{16}$F, the same value as in Ref. [5] ($q = 0.95$), which is consistent with the total experimental $\mu$-capture rate to unbound states, is used (see Table B1 of Ref. [24]). The cross section for $^{16}$O is reduced by about 50% at $E_\nu < 20$ MeV and 30% (20%) around $E_\nu = 30$ (40) MeV compared with that in Ref. [5], where $q = 0.95$ is adopted for all the transitions. The cross section for $^{18}$O is larger than that for $^{16}$O due to the large contribution from the GT transitions in $^{18}$O. Even if 0.205% for the isotope abundance of $^{18}$O is taken into account, the cross section for $^{18}$O is still larger at low neutrino energies, $E_\nu \leq 25$ MeV. Calculated cross sections for $^{18}$O with 0.205% abundance are consistent with those obtained in Ref. [8] (see Fig. 1). They are also comparable to the $\nu_e$-$e^-$ elastic cross sections at $E_\nu \geq 20$ MeV, and even larger at $E_\nu > 50$ MeV. Calculated cross sections for $^{16}$O ($\bar{\nu}_e$, e$^+$) $^{16}$N are also shown in Fig. 4 (right panel). The cross section obtained with $q = 0.68$ (solid curve) for the transition to the first $0^-$, $1^-$ and $2^-$ states in $^{16}$N is reduced by about half at $E_\nu \leq$ 20 MeV compared with that obtained with $q$ =0.95 [5]. We also notice by comparing to Fig. 3

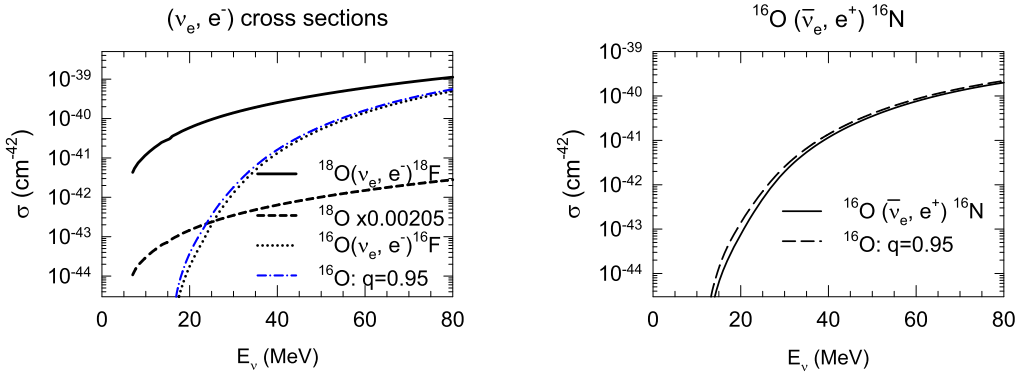


Fig. 4. (Left) Comparison of $(\nu_e, e^-)$ total cross sections for $^{18}$O and $^{16}$O. The dotted curve is obtained by the shell model with the use of $q = 0.68$ for the quenching of $g_A$ for the transitions to the first $0^-$, $1^-$ and $2^-$ states of $^{16}$F. The dash-dotted curve is taken from Ref. [5], where $q = 0.95$ is used. The dashed curve denotes the cross section for $^{18}$O, where 0.205% isotope abundance of $^{18}$O is taken into account. (Right) Cross sections for $^{16}$O $(\bar{\nu_e}, e^+)$ $^{16}$N obtained by shell-model calculations. Solid curve is obtained with $q = 0.68$ for the transitions to the first $0^-$, $1^-$ and $2^-$ states of $^{16}$N, while dashed curve is obtained with $q = 0.95$ [5].

that the cross section for $^{16}$O is larger than that for $^{18}$O by one-order of magnitude in the $(\bar{\nu_e}, e^+)$ channel.

Contributions to the $(\nu_e, e^-)$ cross sections from $^{18}$O and $^{16}$O in water are compared for $E_\nu =$ 10, 20 and 30 MeV in Fig. 5 as functions of the kinetic energy of the emitted electron, $T_e$. The threshold energy of the detector is taken to be 5 MeV. As the threshold energy of for $^{16}$O $(\nu_e, e^-)$ $^{16}$F reaction is 15.42 MeV, there are no contributions from $^{16}$O below $E_\nu = 20$ MeV. There are contributions from $^{18}$O only at $E_\nu = 10$ MeV. Note that the threshold energy for $^{18}$O $(\nu_e, e^-)$ $^{18}$F reaction is as low as 1.66 MeV. Contributions at $T_e = 8.34$ and 7.30 MeV come from the GT transition to the ground state of $^{18}$F and the IAS, respectively. For $E_\nu = 20$ MeV, a large contribution from $^{18}$O caused by the transitions to the GT and IAS states is seen at $T_e = 18.34$ and 17.30 MeV, while the transition to the ground state of $^{16}$F $(0^-)$ at $T_e = 4.59$ MeV is the only contribution from $^{16}$O. For $E_\nu = 30$ MeV, contributions from $^{16}$O become large at $T_e =$ 7-10 and $\approx$14.3 MeV, but those from $^{18}$O are also noticed in a different energy region at $T_e =$ 27-28 MeV though their magnitude is smaller compared to $^{16}$O. Contributions from $^{18}$O are thus expected to be found at higher $T_e$ region. In particular, they can be observed exclusively below $E_\nu \approx 20$ MeV. The cross sections folded over the decay-at-rest (DAR) $\nu_e$ spectrum are also shown in Fig. 5. There are no contributions from $^{16}$O at $T_e >$37 MeV, while those from $^{18}$O are found at $T_e =$ 37-50 MeV. Thus the contributions from $^{18}$O can be exclusively observed at the higher electron energy region. Note also that $\nu_e$-induced reactions on $^{18}$O have almost isotropic angular distributions, while those on $^{16}$O are backward-peaked [8]. An experiment with DAR $\nu_e$ should be able to measure the cross sections of $^{18}$O and $^{16}$O separately and test the present model calculations [25].

## 3. Effects of $^{18}$O mixture in water on supernova $\nu$ detection

### 3.1. Cross sections folded over supernova neutrino spectra

In order to make an estimate for the supernova neutrino event rate, the folding effects of the $(\nu_e, e^-)$ cross sections over supernova neutrino spectra are investigated. Cross sections for $(\nu_e,$

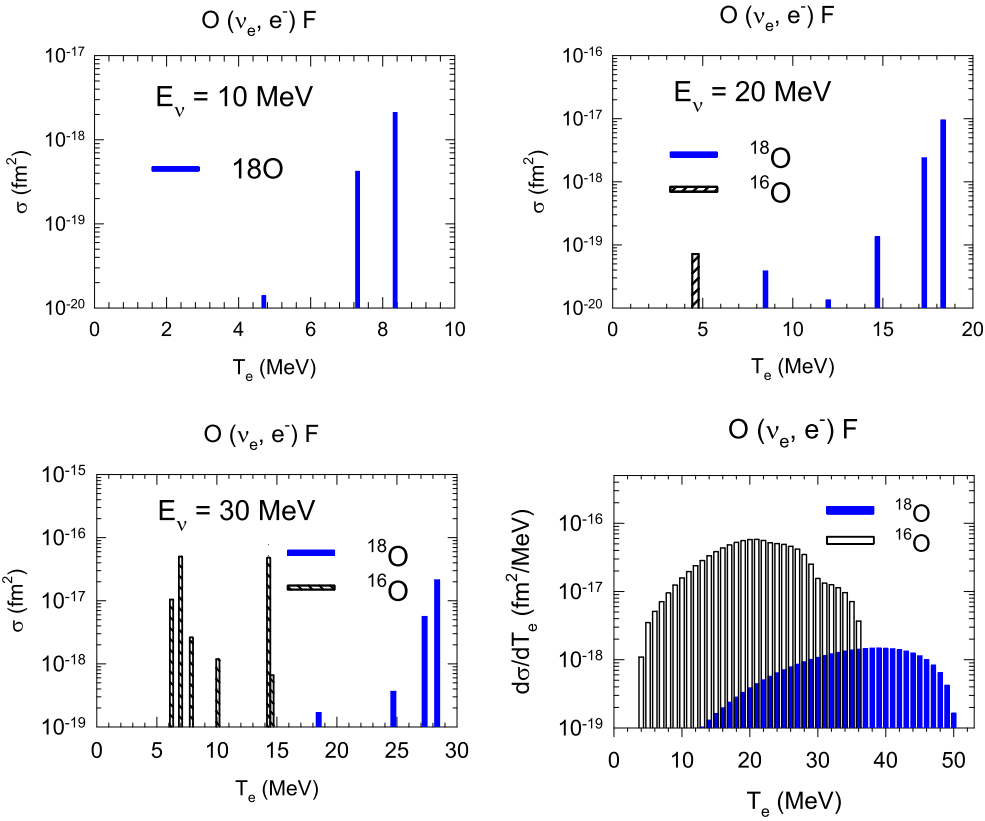


Fig. 5. Contributions from $^{18}$O and $^{16}$O in water to O ($\nu_e$, e$^-$) F cross sections as functions of emitted electron kinetic energy, $T_e$. Cases for $E_\nu = 10$, 20, and 30 MeV, as well as the one folded over the DAR $\nu_e$ spectrum, are shown.

e$^-$) reactions on $^{18}$O and $^{16}$O folded over supernova neutrino spectra as functions of emitted electron energies $T_e$ are shown in Fig. 6. The case of neutrino spectra of a normal supernova obtained by simulations of supernova explosions, denoted as NK1 [24,26], and the case for a modified Maxwell-Boltzmann (mMB) distribution with a neutrino average energy of 10 MeV are shown. The NK1 model is one of the spectral models provided in Supernova Neutrino Database [4] and its progenitor has the mass of $M = 20M_\odot$ and the metallicity of $Z = 0.02$. For the mMB, the following parametrization is adopted with $\alpha = 3$ [18]:

$$f(E_\nu) = \frac{(\alpha+1)^{\alpha+1}}{\Gamma(\alpha+1)\langle E_\nu\rangle^{\alpha+1}} E_\nu^\alpha \exp(-\frac{(\alpha+1)E_\nu}{\langle E_\nu\rangle}) \tag{5}$$

where $\langle E_\nu\rangle$ is average neutrino energy. The neutrino spectra for NK1, mMB, and Fermi-Dirac distributions are shown in Fig. 6 (lower panel). One notices that there remain more high-energy components in the spectrum of NK1 compared with the others. The spectrum for mMB damps more rapidly in the high energy region for a larger value of the pinching parameter, $\alpha$. As $T_e$ increases, the cross sections folded over the NK1 spectra decrease more slowly compared with those of the mMB spectra for both $^{18}$O and $^{16}$O. This is due to a large high energy component that remains up to $E_\nu \approx 100$ MeV in the spectra of NK1. Higher energy electrons are expected to be emitted more for the NK1 spectra. The cross sections for $^{18}$O and $^{16}$O are comparable up to

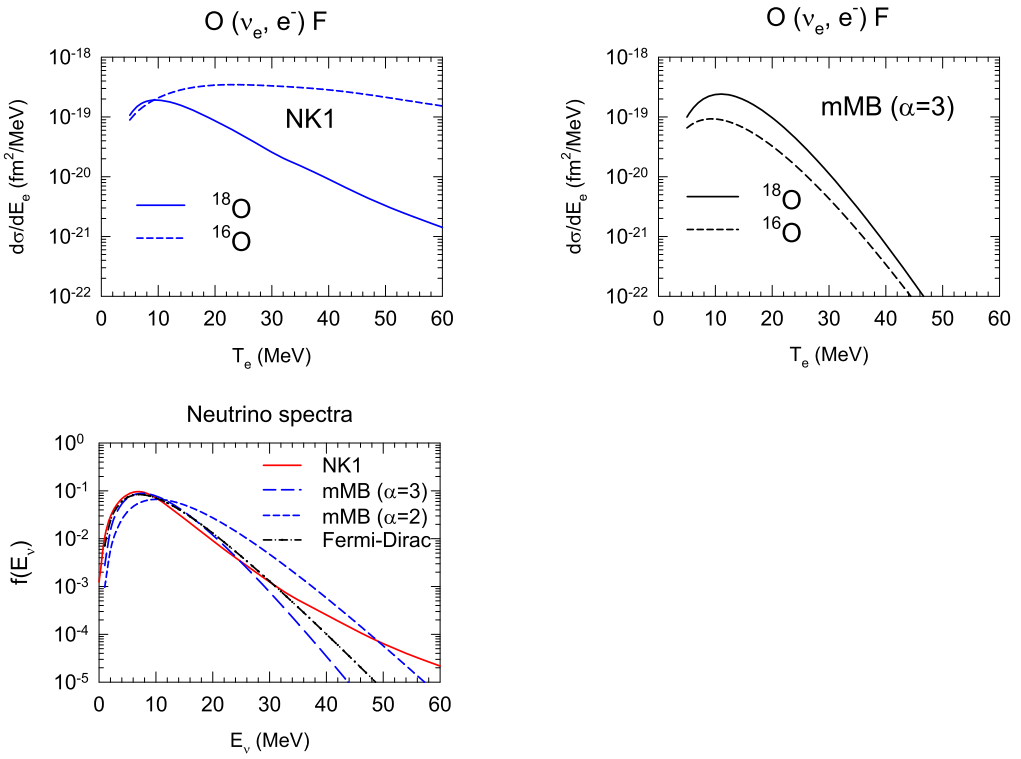


Fig. 6. Cross sections for ($\nu_e$, e$^-$) reactions on $^{18}$O and $^{16}$O as functions of emitted electron energies, $T_e$. Neutrino spectra of a normal supernova, NK1 [26,4], and modified Maxewll-Boltzmann (mMB) distributions with $\alpha = 3$ and neutrino average energy of 10 MeV are adopted for left and right panels, respectively. The normalized neutrino spectra for the cases of NK1 ($\nu_e$), mMB distributions with $\alpha = 3$ and 2, and Fermi-Dirac distribution for $T = 3.2$ MeV used in Table 1 are also shown (lower panel). The average neutrino energies are 9.32 MeV for the NK1 spectrum and 10.1 MeV for the mMB and the Fermi-Dirac distributions.

$T_e \approx$10 MeV, but those for $^{16}$O are more enhanced compared to $^{18}$O at higher $T_e$ regions for the NK1 case. In the case of the mMB spectra, on the other hand, the cross sections for $^{18}$O and $^{16}$O are comparable up to $T_e \approx 50$ MeV, but their magnitudes decrease more rapidly as $T_e$ increases. This indicates that contributions from $^{18}$O are non-negligible and can affect the count rate for supernova $\nu$ events in water Cherenkov detectors. As the high energy component contributes more to the events on $^{16}$O than on $^{18}$O for the NK1 spectra, the $^{18}$O admixture can affect the event rate less than the case for the mMB spectra.

### *3.2. Supernova ν event rates in water Cherenkov detectors*

In this subsection, we estimate the event rates for supernova $\nu$ detection by using the neutrino spectra given by NK1, mMB, and Fermi-Dirac distributions. For this purpose, a supernova at 10 kpc and the detection at 32 kton water Cherenkov detector, Super-Kamiokande, are assumed. Furthermore, cases with and without the Mikheyev-Smirnov-Wolfenstein (MSW) neutrino oscillations [27] are considered. The neutrino number spectrum for $\nu_e$ is given by [26]

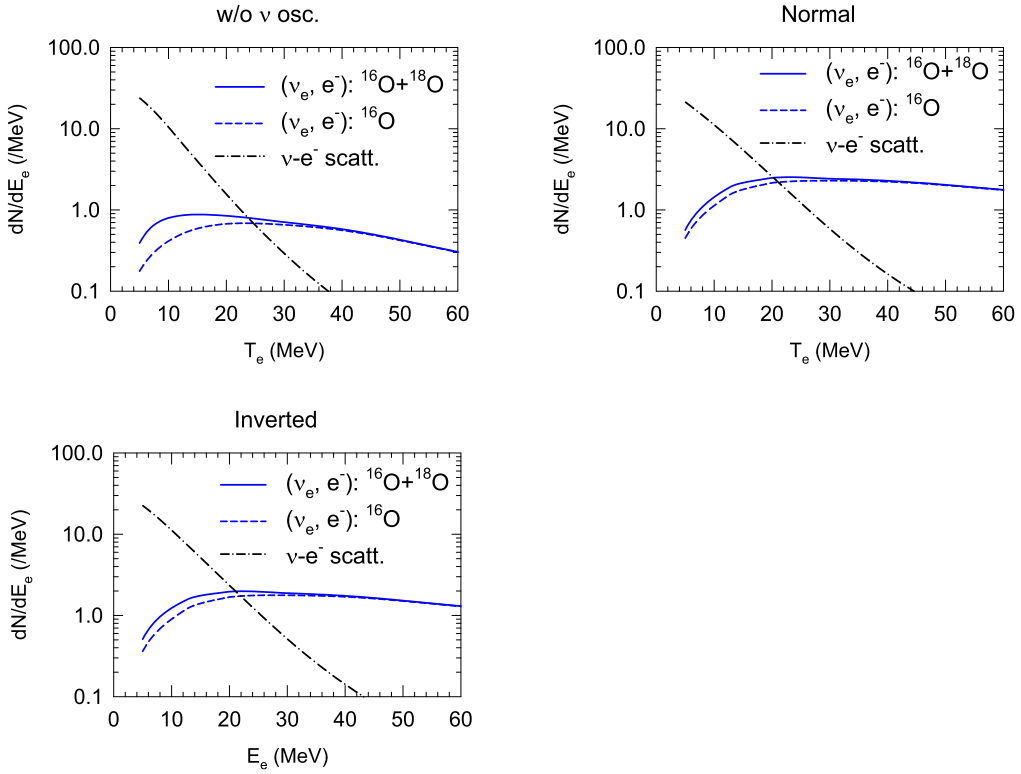


Fig. 7. Event spectra for the supernova model, NK1 [26,4], as functions of emitted electron energy $T_e$ for the cases without $\nu$ oscillations (left), with the normal hierarchy hypothesis (center) and with the inverted hierarchy hypothesis (right). Solid and dashed curves correspond to ($\nu_e$, $e^-$) reactions on $^{16}$O + $^{18}$O with 0.205% and on $^{16}$O only, respectively. Dash-dotted curves correspond to elastic $\nu$+$e^-$ scattering.

$$\frac{dN_{\nu_e}(E_\nu)}{dE_\nu} = P\frac{dN^0_{\nu_e}(E_\nu)}{dE_\nu} + (1-P)\frac{dN^0_{\nu_x}(E_\nu)}{dE_\nu} \tag{6}$$

where $P$ is the survival probability of $\nu_e$ and $\frac{dN^0_{\nu_i}}{dE_\nu} = \frac{E_{\nu_i,\mathrm{total}}}{\langle E_{\nu_i}\rangle} f(E_{\nu_i})$ with $i = e$ and $x$ ($x = \mu$, $\tau$, $\bar{\mu}$, and $\bar{\tau}$) are neutrino number spectra before the oscillations. $E_{\nu_i,\mathrm{total}}$ is the total energy emitted by $\nu_i$, $\langle E_{\nu_i}\rangle$ is the average energy for $\nu_i$ and $f(E_{\nu_i})$ is the normalized neutrino spectrum for $\nu_i$. The value of $P$ is taken to be 0 and 0.32 for normal hierarchy (NH) and inverted hierarchy (IH), respectively [28]. Similar estimations were done in Ref. [26], but only $^{16}$O was taken into account.

Here, we study the possible effects of $^{18}$O mixture in water Cherenkov detectors on the event rates of supernova neutrinos. Firstly, we consider the neutrino spectra of NK1 model, whose averaged neutrino energies for $\nu_e$, $\bar{\nu}_e$ and $\nu_x$ are 9.32, 11.1 and 11.9 MeV, respectively [4]. Event spectra for ($\nu_e$, $e^-$) reactions on $^{16}$O only and on $^{16}$O + $^{18}$O with 0.205% abundance as well as for elastic $\nu$-$e^-$ scattering are shown in Fig. 7 for the cases without $\nu$ oscillations and with oscillations for NH and IH. For $\nu$-$e^-$ scattering, $\nu$ includes all flavors, $\nu_e$, $\bar{\nu}_e$, $\nu_\mu$, $\bar{\nu}_\mu$, $\nu_\tau$ and $\bar{\nu}_\tau$. In case without the oscillation, the contribution from $^{18}$O enhances the spectra for $^{16}$O by about

Table 1
Results for expected event numbers for ($\nu_e$, e$^-$) reaction for a normal supernova [26] (see text) are given in the row denoted as NK1. The threshold energy of the detector is taken to be 5 MeV. Cases without neutrino oscillations, with the MSW oscillations with normal and inverted hierarchies, are given for pure $^{16}$O and $^{16}$O with $^{18}$O mixture. Numbers in the bracket denote ($\langle E_{\nu_e}\rangle$, $\langle E_{\nu_x}\rangle$) in units of MeV. Expected event numbers for elastic $\nu$-$e^-$ scattering for the NK1 spectra are given in the first row [26], where, $\nu$ includes all flavors. Neutrino spectra of modified Maxwell-Boltzmann (denoted as mMB) and Fermi-Dirac distributions are also used for the estimation of the event numbers. Numbers in the brackets for the mMB distributions denote ($\langle E_{\nu_e}\rangle$, $\langle E_{\nu_x}\rangle$) in units of MeV and ($\alpha$ for $\nu_e$, $\alpha$ for $\nu_x$). Those for the Fermi-Dirac distributions denote ($T_{\nu_e}$, $T_{\nu_x}$) in units of MeV. The chemical potential is taken to be 0 for the Fermi-Dirac distributions.

| Neutrino spectra | Target | No oscillation | Normal | Inverted |
|---|---|---|---|---|
| NK1 [4] | $\nu$+$e^-$ $\rightarrow$ $\nu$+$e^-$ | 140 | 157 | 156 |
| NK1 [4] | $^{16}$O | 36 | 156 | 118 |
| (9.32, 11.9) | $^{16}$O +$^{18}$O | 42 | 165 | 126 |
| mMB [29] | $^{16}$O | 4 | 63 | 44 |
| (10.14, 12.89) | $^{16}$O +$^{18}$O | 11 | 76 | 55 |
| $\alpha$=(2.90, 2.39) | | | | |
| mMB | $^{16}$O | 14 | 50 | 39 |
| (12, 14.6) | $^{16}$O +$^{18}$O | 22 | 61 | 48 |
| $\alpha$=(2.9, 2.9) | | | | |
| mMB | $^{16}$O | 57 | 419 | 303 |
| (11.0, 15.8) | $^{16}$O +$^{18}$O | 70 | 439 | 321 |
| $\alpha$=(2, 2) | | | | |
| mMB | $^{16}$O | 6 | 67 | 48 |
| (11.0, 15.8) | $^{16}$O +$^{18}$O | 13 | 78 | 57 |
| $\alpha$=(3, 3) | | | | |
| mMB | $^{16}$O | 33 | 128 | 98 |
| (10.1, 12.6) | $^{16}$O +$^{18}$O | 45 | 144 | 112 |
| $\alpha$=(2, 2) | | | | |
| mMB | $^{16}$O | 3 | 16 | 12 |
| (10.1, 12.6) | $^{16}$O +$^{18}$O | 9 | 24 | 19 |
| $\alpha$=(3, 3) | | | | |
| Fermi-Dirac [14,30] | $^{16}$O | 13 | 110 | 78 |
| (3.5, 5) | $^{16}$O +$^{18}$O | 20 | 121 | 88 |
| Fermi-Dirac | $^{16}$O | 7 | 30 | 23 |
| (3.2, 4) | $^{16}$O +$^{18}$O | 13 | 39 | 31 |

60% at $T_e < 20$ MeV. A mild enhancement of the spectra by 20-30% from $^{18}$O admixture is noticed at $T_e \leq$25 MeV for the case with the oscillations.

Expected event numbers estimated for the ($\nu_e$, e$^-$) reaction for pure $^{16}$O and for $^{16}$O with 0.205% mixture of $^{18}$O are shown in Table 1 for the case with and without the MSW matter oscillation effects [28,4]. Both NH and IH are considered for the MSW oscillations. The event numbers for elastic $\nu$-$e^-$ scattering are also given in Table 1 for comparison. Note that the event numbers for pure $^{16}$O in Table 1 are different from those in Ref. [26]. This is because we adopt the quenching factor for $g_A$ of $q = 0.68$ for the transitions from $^{16}$O to the first $0^-$, $1^-$ and $2^-$ states in $^{16}$F [24], while it was taken to be $q = 0.95$ in Ref. [26].

In the case of the NK1 neutrino spectra, the event numbers are found to be enhanced by 17% and 6-7% with the $^{18}$O admixture for the case without the oscillation and with the oscillation, respectively. Note that the $^{18}$O mixture becomes more important at lower $\nu_e$ energy region. In the case with the oscillations, the energy of $\nu_e$ is higher than the case without the oscillations as

high energy $\nu_x$'s are converted to $\nu_e$, and the effects of $^{18}$O mixture become less than the case without the oscillation. The change of event numbers due to the $^{18}$O mixture is found to be rather modest, by 6-9 counts, because of the characteristic behavior of the neutrino spectra of NK1, whose strengths remain in the high energy region, $E_\nu > 50$ MeV. The high energy component is produced in the accretion phase of supernova explosions [4]. Due to the enhancement by effects of the neutrino oscillations, the event numbers become comparable to those of the elastic $\nu$-$e^-$ scattering, which is particularly important to detect the direction of the supernova within 3 to 5 degrees [1]. However, the $^{18}$O admixture would not affect the accuracy of the direction since the effect is not large enough to cover up the contributions from the $\nu$-$e^-$ elastic scattering below $T_e \approx$20 MeV (Fig. 7). Furthermore, the $\nu$-$e^-$ elastic scattering has sharply forward-peaked angular distributions, while $\nu_e$-induced reactions on $^{18}$O and $^{16}$O have almost isotropic and mildly backward-peaked angular distributions, respectively. The measurement of $\nu$-$e^-$ elastic scattering remains an important method to determine the direction of the neutrino source.

Next, we consider neutrino spectra with analytic forms. In the following, total neutrino energy of $3.2 \times 10^{52}$ erg/flavor is assumed. Results for the neutrino spectra of modified Maxwell-Boltzmann (mMB) and Fermi-Dirac distributions are also given in Table 1. For mMB, the spectra of Ref. [29] obtained at 1016 ms for the postbounce time for a spherically symmetric supernova model, and those that satisfy a relation $\langle E_{\nu_x}\rangle/\langle E_{\nu_e}\rangle \approx$1.22 [18] are used. While the change of the expected event numbers with the $^{18}$O admixture is modest, by 7-13 counts, similar to the case of NK1, the percentage of increase is larger than that of NK1 for both the cases with and without the oscillations. In particular, for the spectra of Ref. [29], it is 175% for the case without the oscillations. For the late phase at 1016 ms after the bounce, the emission of high-energy $\nu_e$ is suppressed, which is reflected in a large value of the pinching parameter in the spectrum, $\alpha = 2.90$. Thus, the impact of the $^{18}$O admixture is notable due to the reactions with low-energy neutrinos for the case without the oscillations. For the case with the oscillations, the event numbers become larger similar to the case of NK1 because $\nu_x$'s, which are converted to $\nu_e$'s, have a spectrum with high average energy and small $\alpha$ value.

In order to look into the dependence on parameters, two cases for the average energies, $(\langle E_{\nu_e}\rangle, \langle E_{\nu_x}\rangle)$ = (11.0, 15.8) and (10.1, 12.6) MeV, are adopted, where $\nu_e$ and $\nu_x$ have the same value of $\alpha$. These average energies correspond to those of the Fermi-Dirac distributions given in Table 1 as explained below. For the pinching parameter, two cases of $\alpha = 2$ and 3 are chosen. As we see from Table 1, the event numbers increase as the neutrino energies increase or the value of $\alpha$ decreases. Increase of the expected event number due to the $^{18}$O admixture is again modest, by 6-20 counts, while the total expected event number for ($\nu_e$, e$^-$) reaction, denoted as $^{16}$O +$^{18}$O in Table 1, are sensitive to the parameters, 9-439 counts. The impact of the $^{18}$O admixture is more notable not only for the case with lower average energy but also for larger $\alpha$ because the spectrum is more pinched (high-energy tail suppressed) for larger $\alpha$ as shown in Fig. 6 (lower panel).

For the Fermi-Dirac distribution, spectra with $(T_{\nu_e}, T_{\nu_x})$ = (3.5, 5) MeV is adopted. $T_{\nu_x}$ is obtained to be 4.8-6.6 MeV in Ref. [14] and 5.4±1.1 MeV in Ref. [30] to avoid an overproduction of $^{11}$B abundance during the Galactic chemical evolution. The case for $(T_{\nu_e}, T_{\nu_x})$ = (3.2, 4) MeV is also given. Average neutrino energy is related to the temperature by $\langle E_\nu\rangle = 3.15\ T_\nu$ for the Fermi-Dirac distribution. The corresponding average neutrino energies of $(T_{\nu_e}, T_{\nu_x})$ = (3.5, 5) and (3.2, 4) MeV are $(\langle E_{\nu_e}\rangle, \langle E_{\nu_x}\rangle)$ = (11.0, 15.8) and (10.1, 12.6) MeV, respectively, which are the same as those of the mMB distributions adopted above. The latter average energies (10.1, 12.6) MeV are close to or a little larger than those of the NK1 spectra. For each set of the average neutrino energies, the event number for the Fermi-Dirac distribution is between that for $\alpha = 2$ and

3 of the mMB spectra because the Fermi-Dirac distribution is softer than $\alpha = 2$ but harder than $\alpha = 3$ as shown in Fig. 6 (lower panel) (see also Sect. 3.1 of Ref. [26]). In comparison with the NK1 spectra, expected event numbers of Fermi-Dirac distribution with $(T_{\nu_e}, T_{\nu_x}) = (3.2, 4)$ MeV are calculated to be smaller by about 3-5 times despite the fact that the average neutrino energies are close to each other (see Table 1). Higher temperatures or average energies are favored to compensate for the missing high-energy components of the spectra. This tendency is also true for the spectra of mMB distributions with $\alpha \approx 3$. Anyway, the qualitative feature that the event number becomes the largest for the MSW oscillation with the NH remains unchanged.

In the case of a failed supernova with a black hole remnant [26], the effects of $^{18}$O mixture are negligible as the neutrino energies are as high as $T_\nu$ = 6-8 MeV and the contributions from $^{16}$O dominate over those from $^{18}$O. For $(\bar{\nu}_e, e^+)$ reactions, the effects can be neglected because of quite small cross sections for $^{18}$O $(\bar{\nu}_e, e^+)$ $^{18}$N compared to $^{16}$O case.

## 4. Summary

Neutrino-nucleus reactions on $^{18}$O are investigated by shell-model calculations with a Hamiltonian, SFO-tls [21], which was used for the study of $\nu$-induced reactions on $^{16}$O [5]. The GT transitions give important contributions in $^{18}$O $(\nu_e, e^-)$ $^{18}$F reaction contrary to the case of $^{16}$O, where dominant contributions come from the spin-dipole transitions. Charged- and neutral-current reaction cross sections for $^{18}$O are evaluated by the multipole expansion method of Walecka [22] with the use of the quenching of $g_A$ determined from the experimental GT strength obtained by ($^3$He, $t$) reactions [7].

The reaction cross section for $^{18}$O $(\nu_e, e^-)$ $^{18}$F is found to be larger than that for $^{16}$O due to the lower threshold energy (1.66 MeV) than that for $^{16}$O (15.42 MeV), and it remains true for low-energy neutrinos, $E_\nu \leq 20$ MeV, even with the consideration of 0.205% admixture of $^{18}$O in water. Cross sections as functions of emitted electron energies induced by reactions on natural water are investigated at $E_\nu = 10$, 20, and 30 MeV as well as for the decay-at-rest (DAR) $\nu_e$. Events from reactions on $^{16}$O and $^{18}$O are found to take place at different electron energy regions separated by 10-15 MeV. We have thus shown how we can separate the contributions from $^{16}$O and $^{18}$O by the measurements using the DAR $\nu_e$'s and test the calculated cross sections in an experiment in the near future [25].

Possible effects of the $^{18}$O admixture in water Cherenkov detectors on the evaluation of the event rate of supernova neutrinos are examined for both the case with and without the neutrino oscillations. Detection of events from a normal supernova at 10 kpc away for 32 kton water of Super-Kamiokande is assumed.

For the neutrino spectra, NK1 [26], obtained by simulations of supernova explosions, the effects of $^{18}$O admixture on the event numbers are found to be modest, a 6-17% increase of the count numbers. The high energy component of the NK1 spectra, produced in the accretion phase of supernova explosions [4], suppresses the relative importance of the $^{18}$O mixture in water. We have also shown that the effects of the neutrino oscillations are large and enhance the event numbers for the reactions on $^{16}$O and $^{18}$O by 3-4 times, which become comparable to those of the elastic $\nu$-$e^-$ scattering. While these points were noticed by the previous work on $^{16}$O [26], we have confirmed these features of the cross sections and the event rate with the inclusion of $^{18}$O and with the use of more accurate quenching factors ($q$=0.68) for the spin-dipole transitions to the first $0^-$ (g.s.), $1^-$ and $2^-$ states of $^{16}$F [24].

For neutrino spectra of modified Maxwell-Boltzmann (mMB) and Fermi-Dirac distributions with total neutrino energy of $3.2\times10^{52}$ erg/flavor, estimated event numbers are found to depend

sensitively on average energies and pinching parameters, $\alpha$, and they increase by 1.2-3.0 (1.05-1.6) times in case without (with) the neutrino oscillations with the $^{18}$O admixture. In any case, the change of the count numbers is similar but a bit larger than the case of the NK1 spectra; by 6-20 counts. The neutrino oscillations enhance the event numbers considerably, similar to the case of the NK1 spectra. The choice of neutrino spectra is important for a quantitative evaluation of the event numbers.

We have shown for the NK1 spectra, which were obtained from an ordinary supernova neutrino model consistent with SN1987A in the neutrino event number and duration [31], that the contribution from $^{18}$O (0.205% admixture) enhances the event rates from $^{16}$O in the electron spectra below $T_e = 20$ MeV by 60% and 20-30% for the case without and with the neutrino oscillations, respectively. In the latter case, the event rates for $^{18}$O and $^{16}$O become comparable to those of the neutrino-electron scattering, while the rates below $T_e$ =20 MeV are much lower than those of the neutrino-electron scattering, which is important to detect the direction of the next supernova.

## CRediT authorship contribution statement

**Toshio Suzuki:** Evaluations of neutrino-induced reactions on $^{16}$O and $^{18}$O by shell-model calculations; Evaluations of the count rate of supernova neutrino events with water Cherenkov detectors; Ideas for the present work; Writing the manuscript.

**Ken'ichiro Nakazato:** Evaluation of supernova neutrino spectra used in the present work; Selection of supernova spectra adopted in the present work; Writing a part of the manuscript, and editing the manuscript.

**Makoto Sakuda:** Proposal for presenting separate contributions from $^{16}$O and $^{18}$O as functions of emitted electron energies, and the possibility for the measurement; Comparison of neutrino-oxygen reaction cross sections and neutrino-electron scattering cross sections; Editing the manuscript.

## Declaration of competing interest

The authors declare that they have no known competing financial interests or personal relationships that could have appeared to influence the work reported in this paper.

## Data availability

Data will be made available on request.

## Acknowledgements

This work was supported in part by the JSPS KAKENHI, Grant Nos. JP19K03855, JP19H05811, JP20K03973 and JP20K03989. Some part of the results in this paper was presented at the Workshop on "Neutrino Interaction Measurements for Supernova Neutrino Detection" at Oak Ridge National Laboratory. We would like to thank the Oak Ridge National Laboratory and the workshop participants for stimulating discussion.

## References

[1] K. Abe, et al., Astropart. Phys. 81 (2016) 39;

K. Abe, et al., Nucl. Instrum. Methods A 1027 (2022) 166248.
[2] K. Abe, et al., Hyper-Kamiokande Collaboration, Astrophys. J. 916 (2021) 15;
K. Abe, Ke. Abe, H. Aihara, et al., Hyper-Kamiokande Design Report, arXiv:1805.04163, 2018;
http://www.hyperk.org/.
[3] K.G. Balasi, K. Langanke, G. Martínez-Pinedo, Prog. Part. Nucl. Phys. 85 (2015) 33.
[4] K. Nakazato, K. Sumiyoshi, H. Suzuki, T. Totani, H. Umeda, S. Yamada, Astrophys. J. Suppl. 205 (2013) 2.
[5] T. Suzuki, S. Chiba, T. Yoshida, K. Takahashi, H. Umeda, Phys. Rev. C 98 (2018) 034613.
[6] K. Langanke, P. Vogel, E. Kolbe, Phys. Rev. Lett. 76 (1996) 2629;
E. Kolbe, K. Langanke, P. Vogel, Phys. Rev. D 66 (2002) 013007.
[7] H. Fujita, Y. Fujita, Y. Utsuno, K. Yoshida, T. Adachi, A. Algora, et al., Phys. Rev. C 100 (2019) 034618.
[8] W.C. Haxton, Phys. Rev. D 36 (1987) 2283.
[9] K. Hirata, et al., Phys. Rev. Lett. 58 (1987) 1490.
[10] R. Bionta, et al., Phys. Rev. Lett. 58 (1987) 1494.
[11] R. Mayle, J.R. Wilson, D.N. Schramm, Astrophys. J. 318 (1987) 288.
[12] S.E. Woosley, D.H. Hartmann, R.D. Hoffman, W.C. Haxton, Astrophys. J. 356 (1990) 272.
[13] S.E. Woosley, T.A. Weaver, Astrophys. J. Suppl. 101 (1995) 181.
[14] T. Yoshida, T. Kajino, D.H. Hartmann, Phys. Rev. Lett. 94 (2005) 231101.
[15] T. Yoshida, T. Kajino, H. Yokomakura, K. Kimura, A. Takamura, D.H. Hartmann, Phys. Rev. Lett. 96 (2006) 091101; Astrophys. J. 649 (2006) 319.
[16] T. Hayakawa, S. Chiba, T. Kajino, G.J. Mathews, Phys. Rev. C 81 (2010) 052801.
[17] T. Hayakawa, P. Mohr, T. Kajino, S. Chiba, G.J. Mathews, Phys. Rev. C 82 (2010) 058801.
[18] M.Th. Keil, G. Raffelt, H.-Th. Janka, Astrophys. J. 590 (2003) 971.
[19] A. Siverding, G. Martínez-Pinedo, L. Huther, K. Langanke, A. Heger, Astrophys. J. 865 (2018) 143.
[20] A. Siverding, K. Langanke, G. Martínez-Pinedo, R. Bollig, H.-T. Janka, A. Heger, Astrophys. J. 876 (2019) 151.
[21] T. Suzuki, T. Otsuka, Phys. Rev. C 78 (2008) 061302.
[22] J.D. Walecka, in: V.H. Highes, C.S. Wu (Eds.), Muon Physics, vol. II, Academic, New York, 1975;
J.S. O'Connell, T.T.W. Donnelly, J.D. Walecka, Phys. Rev. C 6 (1972) 719.
[23] T. Suzuki, S. Chiba, T. Yoshida, T. Kajino, T. Otsuka, Phys. Rev. C 74 (2006) 034307.
[24] M. Sakuda, T. Suzuki, M.S. Reen, K. Nakazato, H. Suzuki, Prog. Theor. Exp. Phys. 2023 (2023) 013D02.
[25] D. Akimov, et al., COHERENT Collaboration, The COHERENT program, arXiv:2204.04575 [hep-ex], April 2022.
[26] K. Nakazato, T. Suzuki, M. Sakuda, PTEP 2018 (2018) 123E02.
[27] L. Wolfenstein, Phys. Rev. D 17 (1978) 2369;
L. Wolfenstein, Phys. Rev. D 20 (1979) 2634;
S.P. Mikheyev, A.Y. Smirnov, Sov. J. Nucl. Phys. 42 (1985) 913;
S.P. Mikheyev, A.Y. Smirnov, Sov. Phys. JETP 64 (1968) 4.
[28] K. Nakazato, E. Mochida, Y. Niino, H. Suzuki, Astrophys. J. 804 (2015) 75;
A.S. Dighe, A.Yu. Smirnov, Phys. Rev. D 62 (2000) 033007.
[29] I. Tamborra, B. Muller, L. Hudepohl, H.-T. Janka, G. Raffelt, Phys. Rev. D 86 (2012) 125031.
[30] T. Yoshida, T. Suzuki, S. Chiba, T. Kajino, H. Yokomakura, K. Kimura, A. Takamura, D.H. Hartmann, Astrophys. J. 686 (2008) 448.
[31] Y. Suwa, K. Sumiyoshi, K. Nakazato, Y. Takahira, Y. Koshio, M. Mori, R.A. Wendell, Astrophys. J. 881 (2019) 139.